Impact of Hydrothermal Carbonization Conditions on the Formation of Hydrochars and Secondary Chars from the Organic Fraction of Municipal Solid Waste

Michela Lucian[1], Maurizio Volpe[1], Lihui Gao[2,3], Giovanni Piro[1], Jillian L. Goldfarb[1,2,4,5], Luca Fiori[1*]

1. Department of Civil, Environmental and Mechanical Engineering, University of Trento, via Mesiano 77, 38123 Trento, Italy
2. Department of Mechanical Engineering and Division of Materials Science & Engineering, Boston University, 110 Cummington Mall, Boston, MA 02215, United States
3. School of Chemical Engineering and Technology, China University of Mining and Technology, No.1 Daxue Road, Xuzhou 221116, People's Republic of China
4. Boston University Initiative on Cities, 75 Bay State Road, Boston MA 02215
5. The John and Willie Leone Family Department of Energy & Mineral Engineering, The EMS Energy Institute, Institutes of Energy & the Environment, The Pennsylvania State University, Hosler Building, University Park, PA 16802, USA

Abstract

Managing the vast quantities of municipal solid waste discarded daily around the globe is critical to insuring global environmental health. Hydrothermal carbonization of the organic fraction of municipal solid waste (OFMSW) could mitigate landfill issues while providing a sustainable solid fuel source. This paper demonstrates the impact of processing conditions on the formation and composition of hydrochars and secondary char of OFMSW; harsher conditions (higher temperatures, longer residence times) decrease generally the solid yield while increasing the higher heating value (HHV), fixed carbon, and elemental carbon. Energy yields upwards of 80% can be obtained at both intermediate and high temperatures (220 and 260-280 °C), but the thermal stability and reactivity of the intermediate hydrochars suggest the formation of a secondary reactive char that condenses on the surface of the primary hydrochar. This secondary char is extractable with organic solvents, and is comprised predominantly of organic acids, furfurals and phenols, which peak at 220 and 240 °C, and decrease at higher carbonization conditions. The HHVs of secondary char are significantly higher than those of primary char.

Keywords: Hydrothermal carbonization; municipal solid waste; secondary char; thermal analysis; coalification; HTC

- To whom correspondence should be addressed: luca.fiori@unitn.it

1. Introduction

Global production of municipal solid waste is approximately 1,300 million tons per year [1]; by 2025 annual production will reach 2,200 million tons [2]. A considerable amount of the organic fraction (OF), which accounts for 30-40 % [3] of the total waste, is incinerated or landfilled, low-cost but polluting processes [1]. The remainder undergoes biological treatments such as composting or anaerobic digestion, which are considered more environmentally friendly technologies, but are often not economically viable because of long holding times (20-30 days). In addition, composting has a high energy consumption and CO_2 footprint, with a relatively low product sale price [4]. Anaerobic digestion suffers from complexity of reactor start-up, toxic and inhibiting compounds in the OF, and process instability due to feedstock heterogeneity [1].

To address these issues, technologies such as hydrothermal carbonization (HTC) are attracting considerable attention to treat the organic fraction of municipal solid waste (OFMSW). During hydrothermal carbonization, the wet biomass is reacted in subcritical water at temperatures up to 300 °C [5], at times ranging from a few minutes to several hours [6]. HTC converts organic wastes into a carbon rich material known as hydrochar, which can be used as a solid fuel owing to its high energy density and heating value, and high carbon content, homogeneity and grindability [7,8]. One of the main advantages of hydrothermal processes is that the heterogeneous wet biomass can be processed without preliminary pre-treatment such as separating and drying [9]. For these reasons, HTC is applied to various wet residues, including: grape marc [10], off specification compost [11], olive wastes [6], food wastes [12], digestate [13], sewage sludge [14–16] and banana stalk [17]. Our group recently demonstrated the feasibility of this technology for large-scale development through a comprehensive economic and process analysis [18]. However, despite its potential, the data available on HTC applied to wet, as-received OFMSW are scarce; there is no systematic study on HTC of OFMSW that investigates the influence of process variables on resulting hydrochar formation. Reza et al. [5]

carried out HTC tests on OFMSW pulp mixed with paper, pre-treated by steam autoclaving sterilization. Berge et al. [19] demonstrated the feasibility of HTC of mixed MSW, including paper, food, plastics, glass and metals. Lin et al. [20] tested hydrochar from MSW as solid fuel. Ingelia S.L. [21], a small enterprise commercializing HTC plants, lists data related to the energy properties and composition of hydrochar from OFMSW acquired at one operating condition (220 °C, 8 h).

Hydrochar forms via two pathways: (1) *solid-solid conversion*, in which the hydrochar maintains the original structural elements and morphology of the parent biomass; (2) a*queous phase degradation* of biomass followed by polymerization of organic molecules into a solid phase [6,22,23]. Throughout the literature "primary char" or "char" is often used to describe the hydrochar formed following pathway (1) and "secondary char" or "coke" the amorphous solid formed following pathway (2)[1]. This secondary char is thought to result because of the sequential hydrolysis, dehydration and isomerization during HTC that produces furfurals, and cleavage reactions yielding intermediate organic acids. These dissolved intermediates can lead to precipitation of the furfurals as a secondary organic phase, which polymerize as microspheres [9,23–27]. The spheres can be further carbonized by dehydration reactions, and are soluble in organic solvents such as acetone and methanol [28].

Secondary char formation is thought to be promoted at high carbonization temperatures, solid loadings, and residence times. It is characterized by spherical-like structures that deposit on the carbonaceous primary char. The high carbon content and high heating value of secondary char is of interest for its potential use as a biofuel [6,28]. As reported by Sevilla et al. [29] and Funke et al. [13], the morphology and structure makes secondary char suitable for advanced carbonaceous material applications, including lithium ion batteries [30]. To date, most studies

[1] *As coke is often used to refer to the formation of non-desorbed products on a secondary substrate (i.e. catalyst surface), in this paper we refer to the products of pathway (2), which condense on the original carbonaceous substrate, as "secondary char"*[58]

focus on the application of secondary char obtained from model compounds such as glucose and fructose. However, no one has yet systematically investigated how HTC reaction conditions affect the formation and characteristics of primary versus secondary char obtained from HTC of a heterogeneous organic residual feedstock. The present paper addresses the gaps identified in the literature by studying the influence of temperature, time and solid load on the mass yields and energy properties of the hydrochar produced, as well as the nature of primary versus secondary char formation resulting from the hydrothermal carbonization of OFMSW.

2. Materials and Methods

2.1 Feedstock

Approximately 29 million tons of municipal solid waste are produced annually in Italy [31]. 30 kg of OFMSW was provided by AMNU, a municipal waste management company in Trento, Italy in November 2016. After elimination of some residual packaging and inert material, the biomass was shredded and homogenized using a knife mill. The average moisture content, evaluated by drying overnight in a ventilated oven at 105 °C, was 78%±0.4 wt%. To preserve the biomass, milled samples of ~16 g each were stored individually in sealed plastic bags in a freezer at -34 °C. OFMSW samples were thawed to room temperature prior to carbonization.

The modified van Soest method was used to determine the extractives, holocellulosic and lignin fractions in the feedstock. Samples were dried at 105 °C, and milled and sieved to > 300 µm. The composition was determined using neutral detergent fiber (NDF) to remove extractives, acid detergent fiber (ADF) for hemicellulose, and acid detergent lignin (ADL) for cellulose removal. Klason lignin [32] content was taken as the remaining. This analysis was repeated thrice.

2.2 Hydrothermal Carbonization

The hydrothermal reactions were carried out in a 50 ml stainless steel (AISI 316) batch reactor as described previously [11,33]. A series of experiments were run with reaction time

ranging from 0 to 6 hours, temperatures between 120 and 280 °C, and dry biomass to water ratio (B/W) from 0.05 to 0.25. B/W is the ratio between the dry feedstock and the total water (moisture + additional deionized water). For each experiment, the reactor was loaded with 8 to 16 g ± 0.01 g of wet (as-received) OFMSW and 1 to 28 g ± 0.01 g of deionized water. The choice to use the wet feedstock without any pre-drying may modestly affect the control of B/W, however, this is in agreement with an industrial scale approach. The amount of feedstock and water at each condition was chosen in order to completely cover the biomass with water and leave comparable free volumes (about 40%) in the system during the different runs.

The reactor was purged by flushing with N_2 gas. The system was heated to the desired reaction temperature, and the HTC residence time started when the system reached the set temperature. After the set reaction time, the reactor was quenched by positioning a stainless steel disc at -34 °C at the bottom of the reactor and blowing compressed air into the reactor walls. When the system reached ambient temperature, the volume of gas produced was measured by flowing it into a graduated cylinder [11]. The gas yield was calculated assuming that the gas produced is entirely CO_2; literature shows that CO_2 is always greater than 90 vol.% [10,11]. The condensed phases were filtered using 45 µm cellulose filters. The pH of the aqueous biomass mixture before carbonization and of the liquid after the HTC were measured using a Profi-Line pH 3310 portable pH-meter. The hydrochar was dried in a ventilated oven at 105 °C for at least 8 h. Hydrochar yield was calculated as the mass ratio between hydrochar and raw biomass (dry basis). Gas yield is the mass of gas produced per unit dry raw biomass; liquid yield was determined by difference. Seventeen individual runs were performed at least twice to insure reproducibility. Hydrochars were named as T_t_B/W, where T denotes temperature in °C, t the residence time in hours, and B/W the dry biomass to water ratio, respectively.

2.3 Hydrochar Characterization

The hydrochars' elemental compositions were determined using a LECO 628 analyzer equipped with sulphur module for CHN (ASTM D-5373 standard method) and S (ASTM D-1552 standard method) determination. The oxygen content was determined by difference. Two runs were performed for each sample, and the average values presented. Proximate analyses were carried out on a LECO Thermogravimetric Analyser TGA 701 using a modified ASTM D-3175-89 standard method: dried at 20 °C/min ramp to 105 °C in air, held until constant weight (< ±0.05%); 16 °C/min from 105 °C to 900 °C, hold time 7 min in N_2 (loss due to volatile matter, VM); isothermal hold at 800 °C in air (loss due to fixed carbon, FC), remaining matter attributed to ash. Higher heating values (HHV) of the raw OFMSW and hydrochars were evaluated according to the CEN/TS 14918 standard by means of a LECO AC500 calorimeter. Data were used to calculate the energy yield EY, as:

$$EY = SY * HHV_{HCdb}/HHV_{Rdb} \quad (1)$$

where SY is the solid yield (*i.e.* the hydrochar yield), times the ratio of the HHVs of the hydrochar (HC) to raw (R) sample (both on a dry basis, db).

The thermal stability and reactivity of a subset of hydrochars were determined using a Mettler-Toledo Thermogravimetric Analyzer-Differential Scanning Calorimeter (TGA-DSC-1) measuring mass to the ±0.1 μg and temperature to the ±0.1 °C. Approximately 4-8 mg of sample was placed in a 70 μL alumina crucible and inserted into the TGA at 25 °C. Samples were heated in either high purity nitrogen (stability) or dry air (reactivity) flowing at 50 mL/min (with an additional 20 mL/min flow of N_2 as a balance protective gas). Samples were heated to 110 °C at 10 °C/min and held for 30 min to remove residual moisture. They were then heated to 900 °C at 50 °C/min and held for 30 min to insure complete devolatilization or oxidation of the sample. Derivative thermogravimetric (DTG) curves were made by taking the derivative of the mass fractional conversion, X, defined as:

$$X = \frac{m_i - m_t}{m_i - m_f} \quad (2)$$

with respect to time, dX/dt. In eq. (2), m_i is the initial mass, m_t is the mass at any time, t, and m_f is the final mass after the hold at 900 °C. Measurements were repeated twice.

2.4. Secondary Char Analysis

To explore the nature of the condensed secondary char deposited on the primary char, a series of hydrochars were extracted using acetone and methanol. Acetone is a polar aprotic solvent, with intermediate polarity; methanol is a protic solvent with a strong polarity, and in combination have been shown to remove the condensed solid organic fraction deposited on primary hydrochar [34]. Each hydrochar sample (approximately 1 g) was mixed with 20 mL of acetone in a beaker at room temperature and then filtered; during filtration most of the char was pressed and retained in the beaker, allowing only the liquid to flow through the filter to enhance recovery. This extraction was repeated thrice, followed by the same procedure using 20 mL of methanol, thrice. The extracts were combined and the solvents evaporated via rotary evaporator at 40 °C to yield $HC_{extractable}$. $HC_{non\text{-}extractable}$ was determined by measuring the solid residue (primary char) remaining in the beaker and trapped on the filter paper. The morphological features of these hydrochars were evaluated via SEM analysis using a JEOL IT 300 scanning electron microscope and an EDS Bruker Quantax equipped with a SDDXFlash 630 M detector. Samples were gold coated and analyzed using an accelerating voltage of 20 kV.

To determine how the composition of the secondary char changes as a result of increasing carbonization temperature, a subset of hydrochars were extracted with dichloromethane (DCM) and the extract dried over anhydrous magnesium sulphate, centrifuged, and the supernatant collected. The extract was analyzed on an Agilent 7890B Gas Chromatograph-Mass Spectrometer (GC-MS) using a split ratio of 25:1 with an injection temperature of 250 °C, and helium as a carrier gas at 29 mL/min. The GC oven started at 30 °C, held 10 min, followed by heating at 3 °C/min to 250 °C, with a final hold of 5 min. The interface temperature was 325 °C. Mass spectra were recorded under electron ionization with a source temperature of 230 °C and

quadrupole temperature of 150 °C with a 7-min solvent delay over an m/z range of 0 to 300 amu and 0.1 m/z step size. A set of calibration "marker" compounds was used (each at minimum purity 99%, calibrated with 7 points between 10 and 700 ppm, minimum R^2 value of 0.995 for each). Additional compounds are reported if their NIST-library matches were above 94%, and any relative area differences (area being a direct function of concentration) noted.

The thermal stability and reactivity of a subset of extracted ($HC_{non\text{-}extractable}$) and non-extracted (*i.e.* as-carbonized) hydrochars were analyzed on the TGA as described above. The TGA results of DCM and acetone+methanol extracted hydrochars were indistinguishable, suggesting that the extraction methods were equivalent in terms of removing secondary char. The DCM proved a more suitable solvent for GC-MS analysis in terms of separation of distinct peaks.

3. Results and Discussion

Transforming OFMSW to a renewable fuel would mitigate environmental issues associated with landfilling, while providing a renewable energy source. The elemental composition of the raw OFMSW feedstock used is reported in Table 1. Elemental analysis is in accord with average values reported for OFMSW across 18 cities in 12 countries [1]. Sulphur content was lower than 0.2 wt%. The fiber analysis performed on raw biomass shows a high amount of extractives (58.8 ± 0.9%) resulting from protein, oil, starch and sugar. Hemicellulose and lignin contents are present in considerable amounts (14.4 ± 0.2%, 17.6 ± 0.1%, respectively), while the cellulose content is relatively low (9.1 ± 0.1%), in agreement with the literature [35].

3.1 Effect of Processing Parameters on Solid and Energy Yield

As the severity of the carbonization process increases – that is, as time and/or temperature increase – the degree to which biomass converts to a carbon dense material increases, as documented across the literature [10,36,37]. For OFMSW this is again the case; solid yields decrease as the temperature increases, as shown in Table 1. This decrease in mass

205 with temperature is due to a series of dehydration and decarboxylation reactions. These reactions
206 become more effective at higher temperatures, leading to an increase in the gaseous phase and
207 decreasing solid yield [11,38]. A modestly reverse trend for hydrochar yields was found at higher
208 temperatures; the hydrochar yield decreases at 240 °C, then increases slightly at 260 °C and 280
209 °C, suggesting that amount of solid formed by back-polymerization of the organic compounds
210 from the liquid phase becomes predominant if compared to the degradation of the solid material
211 from the parent biomass [39]. Notably, each experiment was repeated at least twice, with the 240
212 and 280 °C experiments repeated at least thrice each to confirm the observed trend. The gaseous
213 phase yields progressively increase as temperature increases, following a linear trend ($R^2 = 0.98$),
214 starting at 0.03 at 160 °C to 0.17 at 280 °C. Higher residence times favor the formation of higher
215 quantities of water-soluble compounds, consequently increasing the liquid yield and gaseous
216 yields, as shown in Figure 1. Due to the variability of feedstock moisture content, the results
217 regarding B/W could be affected by the difficulty in the control of total water. However, as it is
218 clear from Fig. 1, solid yields are higher at high B/W with respect to lower B/W ratios (0.05,
219 0.10). According to Funke and Ziegler [40], higher concentrations of biomass could enhance the
220 concentration of monomers in the liquid formed during hydrolysis, favoring the chance of
221 polymerization reactions that lead to an increase in solid yields, as demonstrated by other recent
222 works in the literature [6,34,41].

223 Table 1 details the energy yield of the various hydrochars. EY drops upon heating, even
224 with a residence time of zero hours at 220 °C, B/W=0.15, EY = 0.90. This is due to the large
225 biomass decomposition as the reactor heats to the HTC set point. EY is higher at lower
226 temperatures, reaching a maximum at 180 °C (EY=1.00) and follows the trend of solid yield at
227 higher temperatures. At higher residence times ($\leqslant$ 5 h), the hydrochar mass loss is
228 counterbalanced by the enhancement of the HHV, and therefore EY is approximately constant,

as seen in Fig. 1b. As noted here and in the literature, EY increases with B/W ratio, as a result of the increase in hydrochar yield, and enhanced coalification, increasing HHV [6,34].

Our group recently demonstrated, for prickly pear cactus biomass, that multivariate ordinary least square (OLS) linear regression could predict hydrochars' SY (R^2 = 0.966), EY (R^2 = 0.950) and HHV (R^2 = 0.883) as a function of HTC processing conditions. We found that B/W is the only statistically significant predictor of EY ($p < 0.01$) [28]. Applying OLS regression to the present OFMSW data, we find that both temperature and time are indeed statistically significant predictors of HHV (R^2 = 0.951), represented by Eq. 3:

$$HHV\ (MJ/kg) = 0.066*T(°C) + 0.466*t(h) + 7.600*B/W(g/g) + 12.178 \pm 1.154 \quad (3)$$

Unlike for the more homogeneous prickly pear biomass, the SY and EY are not as well represented by a multivariate linear relationship (Table 2), nor are they well represented by bivariate relationships (data available in Supplemental Information, SI). Again, though, B/W is statistically significant in determining EY, while temperature is a key to determining SY. These relationships between SY, HHV and EY result from the compositional changes that occur because of the hydrolysis, dehydration and isomerization reactions that take place during hydrothermal carbonization. Just as SY, HHV and EY are functions of processing parameters, as are the elemental composition and proximate analyses.

3.2. Effect of Processing Parameters on Hydrochar Composition and Thermal Properties

The proximate analysis (Table 1) shows a decrease in the volatile matter (VM) content with increasing residence time, while the fixed carbon (FC) content predictably follows an opposite trend. This effect is due to the stronger coalification at higher residence time, underscored by the progressive increase in the HHV [6]. Also as expected, as the process temperature increases (with the exception of the 120 °C char), the FC content, elemental carbon content and HHV all increase. No trend is immediately evident in varying the B/W ratio in terms of composition, though the HHV value is slightly higher at higher B/W ratios. The standard

deviations of the proximate analyses are lower than 1.8% (analysis repeated at least twice per sample). However, as shown in Fig. 2a, though the VM content tends to decrease with increasing carbonization severity, the thermal stability, as gauged by the peak DTG temperature and mass loss rate in a nitrogen atmosphere, actually decreases as carbonization time and temperature increase. That is, the highest temperature chars (240, 260, 280 °C) show the highest peak reactivity (on the order of 0.0055 s^{-1}) at lowest peak temperature (T_{peak} < 300 °C), even as compared to the raw (initial peak at 0.004 s^{-1} and 340 °C, second peak at 0.0045 s^{-1} and 410 °C) and 220 °C, 0 h, B/W=0.15 (Peak 1: 0.0035 s^{-1}, 350 °C, Peak 2: 0.0065 s^{-1}, 410 °C). This suggests the formation of a secondary char phase, whereby volatile organics are condensing onto the solid primary char during HTC, and devolatilize from the surface of the char during TGA. The second peaks noted for the high temperature chars (0.002 s^{-1}, T>450 °C) resemble secondary peaks noted for many coals, though shifted to slightly lower temperatures [42–44]. A similar trend is noted for DTG curves of oxidation (Fig. 2b), where the raw OFMSW and 120 °C char exhibit lower peak reactivities in air than their higher temperature counterparts. Again, it is suspected that secondary char condensing on the solid surface is responsible for this reactive behavior, as the chars quickly devolatilize from the surface and oxidize in the air at a faster rate.

The elemental content of carbon (C), hydrogen (H), oxygen (O) and nitrogen (N) of raw OFMSW and hydrochars are presented Table 1; standard deviations of ultimate analyses are lower than 1.3%. The sulphur content in the hydrochars was not determined due to its minimal content in the raw biomass (<0.2 wt%). The elemental analysis shows an increase in elemental carbon weight percent with HTC temperature and time. As the van Krevelen diagram (Fig. 3) shows, as carbonization severity increases, the hydrochars more closely resemble coal in terms of elemental composition with decreasing O/C and H/C ratios. By increasing both the HTC residence time and HTC temperature, the hydrochars have lower H/C and O/C ratios, suggesting that dehydration is a dominant reaction during carbonization. However, at higher residence times

and temperatures, decarboxylation shifts the hydrochar towards lower O/C and higher H/C. The C, H and O composition (Fig. 3b) is highly dependent on carbonization temperature. The carbon content increases almost 150% upon carbonization to 280 °C, with a corresponding decrease in oxygen. The weight percent of hydrogen in the hydrochar is fairly comparable to that of the raw OFMSW no matter the temperature (Fig. 3b), time (Fig. 3c) and B/W (Fig. 3d).

These trends are captured by a multivariate linear model, shown in Table 2 (predicted vs. actual plots available in SI). Unlike previous work on prickly pear biomass [28], where R^2 values were fairly low for predicting elemental C, O, and VM and FC, the OFMSW composition was reasonably well predicted ($R^2 > 0.8$ for all variables). For OFMSW, we find that VM and FC contents are determined by both temperature and time, but not by B/W, confirming our observations [28]. Likewise, as temperature and/or time increases, the elemental carbon increases and oxygen decreases, with B/W not having any statistically significant effect on composition.

3.3. Effect of Processing Parameters on Process Water pH

The pH of the HTC process liquids are shown in Table 1. The standard deviations are less than ±0.3 for each value. Upon heating to 220 °C (t=0 h and B/W =0.15) the pH is 3.8; it increases at 0.5 h, and again slightly at 1 h and 3 h. The pH stabilizes to a value of 4.6 at higher residence times. At temperatures up to 180 °C, the liquid fraction becomes progressively more acidic; on the contrary, the pH increases at HTC temperatures higher than 180 °C. These results are consistent with the idea that the organic acids formed during hydrolysis re-polymerize at higher temperatures and residence times, hence leading to higher pH values at 260 and 280 °C. This trend versus temperature was also observed by Ekpo et al. [45] for hydrothermal carbonization of swine manure. The effect of B/W ratio on pH is negligible.

3.4. Analysis of Secondary Char

The DTG curves in Fig. 2 suggest the presence of a separate, more volatile phase within the solid hydrochars that increases as carbonization severity increases, which is thought to be a

304 secondary char. SEM analysis provides qualitative evidence of its presence and the ability to
305 separate it from the primary char via solvent extraction for samples carbonized for 3 h,
306 B/W=0.15. Fig. 4a shows the amorphous, non-porous nature of the raw OFMSW. Even upon
307 carbonization to 180 °C (Fig. 4b), the biomass begins to decompose, opening pores and reducing
308 the initial amorphous regions on the fibrous support. This progression continues at 240 °C,
309 where we begin to see the formation of smaller, highly spherical amorphous deposits on the fiber
310 surface (Fig. 4c). In Fig. 4d, we see that after extraction, many of these spherical particles are
311 removed, leaving a fibrous structure behind. Fig. 4e, a 5000x magnification of the 280 °C
312 carbonized sample, shows these spherical deposits (which cover even more of the surface as
313 temperature increases) are between 3 and 4 μm in diameter, and sometimes fuse with the spheres
314 next to them. The primary char remaining after extraction for the 280_3_0.15 hydrochar (Fig. 4f)
315 shows some pockets where these spherical chars would have decorated the surface, but also
316 pores in a range of sizes, and both fibrous, smooth surfaces and amorphous surfaces, similar to
317 those observed for biomass-derived activated carbons [46]. While the SEM offers qualitative
318 evidence of the presence of a soluble secondary char, a more quantitative approach sheds light on
319 the amount that forms as a function of carbonization temperature.
320 Repeated solvent washing of a series of hydrochars showed that the extractable char was
321 approximately 40 wt% of the total hydrochar at 220 °C, increased to 55 wt% at 240 °C, and
322 decreased to 34-35 wt% at 260 and 280 °C (Table 3). This suggests that the composition of the
323 secondary char changes as temperature increases. Dehydration and decarboxylation of the solid
324 matrix, combined with reactions in the liquid phase and re-deposition onto the solid char increase
325 the overall degree of carbonization. This is highlighted by the heating contents of the extracted
326 and non-extracted chars, their thermal stability and reactivity, morphology, and composition of
327 the extracts. As seen in Table 3, just as the overall hydrochar HHV increases with temperature,
328 so does the HHV for both the $HC_{non\text{-}extractable}$ and $HC_{extractable}$ components. To check the

consistency of the measured HHVs of the hydrochar fractions, the HHVs of the overall ("as-carbonized") HCs were estimated by Eq. (4):

$$HHV_{HCpredicted} = HHV_{HCnon\text{-}extractable} * \omega_{HCnon\text{-}extractable} + HHV_{HCextractable} * \omega_{HCextractable} \quad (4)$$

where ω_{HC} are the mass fractions comprising the "as-carbonized" hydrochar. In Table 3, we see that the $HHV_{HCpredicted}$ values have estimation errors as compared to measured HHV_{HC} of less than 3%, suggesting that the solvent extraction simply separates the two kinds of char without affecting their energy values. The $HC_{non\text{-}extractable}$ are less energetic than the parent HCs ($HHV_{HCnon\text{-}extractable}/HHV_{HC} < 1$). Consistently, $HHV_{HCextractable}$ are higher than HHV_{HC}. Qualitatively, $HC_{non\text{-}extractable}$ appeared by visual observation to be similar to the parent HC, while $HC_{extractable}$ was a tar-like phase. The calorific values for all four $HC_{extractable}$ samples were higher than 34 MJ/kg, and increase modestly as carbonization temperature increases. However, given the lower yield of extractable char, and higher HHV, we might expect that higher temperatures increase condensation and polymerization reactions in the water phase, leading to larger, more energy intensive products that deposit on the primary char, and fewer volatile components remaining in the solid matrix. This supposition is supported by the thermal analysis.

From the DTG curves of devolatilization, we see that at low temperatures (Fig. 5a) the 120 °C hydrochar's solid remaining after extraction has a similar shape, but more rapid devolatilization rate than the "as-carbonized" char. Such low treatment temperatures do not initiate the series of reactions that define hydrothermal carbonization; cellulosic and lignin-like components will not begin to chemically break down at this point, such that the decomposition may only be of simple sugars and amino acids that are soluble in the process water. Warm water treatment has been shown to physically weaken cellulosic structures, making such pre-treated biomass easier to pyrolyze at lower temperatures and more reactive (e.g. higher DTG peaks) [47], which may explain the observed behavior. When the HTC temperature is increased to 220 °C, we find that the as-carbonized hydrochar has lower thermal stability than its post-extracted

counterpart. That is, the as-carbonized "raw" char devolatilizes faster and at lower temperatures than the extracted solid; the extracted components have higher volatility than the "primary" or non-extracted char. This trend is enhanced as carbonization temperature increases (Fig. 5b). For the 240, 260 and 280 °C samples, the as-carbonized chars have higher peak devolatilization rates (on the order of 0.005 s^{-1}) at lower temperatures (~275-290 °C) than their extracted counterparts, which all peak around 0.0035 s^{-1} and at ~450 °C. This might suggest that the primary (non-extractable) chars remaining after HTC at higher temperatures are not substantially different in terms of composition and structure given the similarities in DTG devolatilization profiles.

However, the oxidation behavior belies a more complex story; the oxidative DTG profiles of the as-carbonized chars all show primary DTG peaks at 0.004 s^{-1} around 235 °C (Fig.s 5c and d). This is likely due to similar reactivities of the extractable char initiating oxidation of the solid char. The post-extracted samples suggest, contrary to the results in N_2, that the reactivities of the primary chars are considerably different from each other. Looking at Fig.s 5c and 5d, all the extracted primary chars display at least two large DTG peaks, one at a lower temperature (ranging from 280-350 °C) and the second between 500-650 °C. This second peak DTG temperature decreases as the HTC temperature decreases, suggesting that increasing HTC temperature enhances destruction of the solid matrix. There is a vast literature concerning biomass pyrolysis and oxidation that demonstrates multiple decomposition regimes that correspond to hemicellulose, cellulose, and lignin components [48]. Analogously, as observed here, different components are hydrolyzed as the severity of carbonization increases, and those remaining are shown through distinct DTG peaks [40].

The varying nature of the post-extracted solid hydrochars is mirrored in the analysis of "secondary" char extracts via GC-MS (Table 4; chromatograms available in SI). There is a stark contrast between the compounds extracted from the 120_3_0.15 hydrochar and those produced at 220 and 260 °C. For example, lauryl lactone is found only in the low temperature char; this

compound is known to form from bacteria present in MSW [49,50], and via oxidation of carbonyls [50,51], and it was found in the extract of the raw OFMSW. In addition, 2-hexene is only detected in the raw OFMSW and 120 °C char, which could form from simple alkenes [52], common by-products of OFMSW fermentation [53]. Also detected in the raw and 120 °C extracts was hexanal, which may result from oxidation of the lipids in OFMSW [54], though itself is an alkyl aldehyde used as flavoring. Pentanal (also a flavoring and founding in olive and spice oils) was found in the raw, 120_3_0.15 and 220_1_0.15 extracts, but not at higher temperatures or residence times. The concentrations of the pentanal and hexanal were both higher in the hydrochars versus the raw sample, suggesting that either the milder carbonization helps "release" the compounds from the solid matrix and/or is responsible for their formation.

At higher temperatures (220, 260 °C), the extracts have large quantities of organic acids, including hexadecanoic and octadecanoic acids. These acids form above 160 °C from the hydrolysis and polymerization of sugars to furfurals to acids and alcohols [55]. As noted in Table 4, at 220 °C, the concentration of octadecanoic acid slightly decreases as residence time increases, starting from 87.6 mg/g_{char} extracted for the 220_1_0.15 char, decreasing to 10.2 mg/g_{char} when the carbonization temperature is raised to 260 °C for 3 hours. This trend of decreasing concentration versus temperature extends to hexadecanoic acid (shown as normalized chromatogram area, total ion count/g_{solid} in Table 4).

Phenols can follow from lignin hydrolysis and, eventually, glucose degradation pathways with furfural intermediates [56]. Lignin is known to be relatively stable: high residence times and temperatures favor its decomposition, as observed here. Specifically, the concentration of phenol increases from 0.56 mg/g_{char} at 220_1_0.15 to 4.44 mg/g_{char} for 260_3_0.15, with a corresponding decrease in the concentration of furfurals. In the presence of water, small acids decompose via decarboxylation reactions, forming CO_2 and H_2 gas [57], which explains the increase in gas yield noted at harsher carbonization conditions. Though acetic acid is an endpoint

in many hydrothermal reactions, forming from glyceraldehydes [55], we do not detect it in the extracted chars, likely due to its higher water solubility retaining it in the water phase. These "secondary char" components could represent platform chemicals for integrated biorefineries.

Overall, the secondary char analysis data suggests that the yield and reactivity of extractable or "secondary" char is maximized at moderate carbonization temperatures between 220 and 240 °C. At these temperatures the extractable yield (Table 3) is highest and the thermal stability and reactivity of the as-carbonized chars are highest (Figure 5). Larger quantities of organic acids and furfurals are extracted from the char at these carbonization conditions, suggesting that at more harsh conditions these components may re-polymerize into the solid primary char as more "coke-" or "coal-like" carbon, rather than remaining as amorphous extractable secondary char. This behavior could explain both the relative amount of extractable and non-extractable char (Table 3) and the slight increase in hydrochar yield at the highest temperatures (260 and 280 °C, Table 1).

Conclusions

The present work systematically investigates the potential to use hydrothermal carbonization (HTC) to upgrade the organic fraction of municipal solid waste (OFMSW) to energy or by-products from "as-received" feedstocks. Despite the perceived heterogeneity of such feedstocks, clear trends emerge in terms of the impact of carbonization conditions on overall and "secondary" char formation. As the severity of carbonization increases – that is, at higher temperatures and longer residence times – the yield and volatile matter content of the hydrochar generally decrease, whereas the elemental carbon content increases, leading to an overall increase in higher heating values. However, at carbonization temperatures above 260 °C, the amount of extractable "secondary" char decreases, after an initial increase at 220-240 °C. The surface of the as-carbonized hydrochars are dotted with amorphous carbon, comprised of organic acids, phenols and furfurals. Some of these compounds decrease at higher HTC temperatures,

perhaps undergoing a re-polymerization and condensation into the solid matrix, whereas others such as phenol increase, probably due to increasing carbonization of the lignin components.

OFMSW hydrochars have the potential to be used as a solid fuel, either alone or co-fired with biomasses or coals. Hydrochars produced at temperatures greater than 220 °C have heating values similar to lignite and sub-bituminous coals, though the presence of the secondary char phase does increase oxidative reactivity and reduce thermal stability, which could lead to lower temperature ignition and reduced boiler efficiency. However, if this secondary char were extracted, it could be used as a source of biorefinery platform chemicals, while the remaining primary or non-extractable char has thermal properties very similar to those of coal, and may represent a better solid fuel alternative in existing boilers.

Acknowledgements

J. Goldfarb acknowledges support of the U.S.-Italy Fulbright Commission and the Boston University Initiative on Cities. L. Gao acknowledges support of the China Scholarship Council.

References

[1] Campuzano R, González-martínez S. Characteristics of the organic fraction of municipal solid waste and methane production: A review. Waste Management 2016;54:3–12. doi:10.1016/j.wasman.2016.05.016.

[2] Al Seadi T, Owen N, Hellstrom H, Kang H. Source separation of MSW. IEA Bioenergy; 2013.

[3] European Environmental Agency. Managing municipal solid waste - a review of achievements in 32 European countries. Copenhagen, Denmark: 2013.

[4] Alibardi L, Cossu R. Composition variability of the organic fraction of municipal solid waste and effects on hydrogen and methane production potentials. Waste Management 2015;36:147–55. doi:10.1016/j.wasman.2014.11.019.

[5] Reza MT, Coronella C, Holtman KM, Franqui-Villanueva D, Poulson SR. Hydrothermal Carbonization of Autoclaved Municipal Solid Waste Pulp and Anaerobically Treated Pulp Digestate. ACS Sustainable Chemistry & Engineering 2016;4:3649–58. doi:10.1021/acssuschemeng.6b00160.

[6] Volpe M, Fiori L. From olive waste to solid biofuel through hydrothermal carbonisation : The role of temperature and solid load on secondary char formation and hydrochar energy properties. Journal of Analytical and Applied Pyrolysis 2017;124:63–72. doi:10.1016/j.jaap.2017.02.022.

[7] Kambo HS, Dutta A. Strength, storage, and combustion characteristics of densified lignocellulosic biomass produced via torrefaction and hydrothermal carbonization. Applied Energy 2014;135:182–91. doi:10.1016/j.apenergy.2014.08.094.

[8] Liu Z, Quek A, Hoekman SK, Balasubramanian R. Production of solid biochar fuel from waste biomass by hydrothermal carbonization. Fuel 2013;103:943–9. doi:10.1016/j.fuel.2012.07.069.

[9] Libra JA, Ro KS, Kammann C, Funke A, Berge ND, Neubauer Y, et al. Hydrothermal carbonization of biomass residuals: a comparative review of the chemistry, processes and applications of wet and dry pyrolysis. Biofuels 2011;2:71–106. doi:10.4155/bfs.10.81.

[10] Basso D, Patuzzi F, Castello D, Baratieri M, Cristina E, Weiss-hortala E, et al. Agro-industrial waste to solid biofuel through hydrothermal carbonization. Waste Management 2016;47:114–21.

[11] Basso D, Weiss-hortala E, Patuzzi F, Castello D, Baratieri M, Fiori L. Hydrothermal carbonization of off-specification compost : A byproduct of the organic municipal solid waste treatment. Bioresource Technology 2015;182:217–24. doi:10.1016/j.biortech.2015.01.118.

[12] Li L, Diederick R, Flora JR V, Berge ND. Hydrothermal carbonization of food waste and associated

packaging materials for energy source generation. Waste Management 2013;33:2478–92. doi:10.1016/j.wasman.2013.05.025.
[13] Funke, Axel, Reebs, Felix, Kruse A. Experimental comparison of hydrothermal and vapothermal carbonization. Fuel Processing Technology 2013. doi:10.1016/j.fuproc.2013.04.020.
[14] Zhai Y, Liu X, Zhu Y, Peng C, Wang T, Zhu L, et al. Hydrothermal carbonization of sewage sludge : The effect of feed-water pH on fate and risk of heavy metals in hydrochars. Bioresource Technology 2016;218:183–8. doi:10.1016/j.biortech.2016.06.085.
[15] Parshetti GK, Liu Z, Jain A, Srinivasan MP, Balasubramanian R. Hydrothermal carbonization of sewage sludge for energy production with coal. Fuel 2013;111:201–10. doi:10.1016/j.fuel.2013.04.052.
[16] Peng C, Zhai Y, Zhu Y, Xu B, Wang T, Li C. Production of char from sewage sludge employing hydrothermal carbonization: Char properties , combustion behavior and thermal characteristics. Fuel 2016;176:110–8. doi:10.1016/j.fuel.2016.02.068.
[17] Upneja A, Dou G, Gopu C, Johnson CA, Newman A, Suleimenov A, et al. Advances Sustainable waste mitigation : biotemplated nanostructured ZnO for photocatalytic water treatment via extraction of biofuels from hydrothermal carbonization of banana stalk. RSC Advances 2016;6:92813–23. doi:10.1039/C6RA21663C.
[18] Lucian M, Fiori L. Hydrothermal Carbonization of Waste Biomass: Process Design, Modeling, Energy Efficiency and Cost Analysis. Energies 2017;10:211. doi:10.3390/en10020211.
[19] Berge ND, Ro KS, Mao J, Flora JR V, Chappell MA, Bae S. Hydrothermal Carbonization of Municipal Waste Streams. Enviromental Science & Technology 2011;45:5696–703. doi:10.1021/es2004528.
[20] Lin Y, Ma X, Peng X, Yu Z, Fang S, Lin Y, et al. Combustion, pyrolysis and char CO2-gasification characteristics of hydrothermal carbonization solid fuel from municipal solid wastes. Fuel 2016;181:905–15. doi:10.1016/j.fuel.2016.05.031.
[21] NEWAPP - Industrial Scale Hydrothermal Carbonization: new applications for wet biomass waste. 2016.
[22] Kruse A, Koch F, Stelzl K, Zeller M. Fate of Nitrogen during Hydrothermal Carbonization. Energy&Fuels 2016:6–11. doi:10.1021/acs.energyfuels.6b01312.
[23] Karayildirim T, Sınag A, Kruse A. Char and Coke Formation as Unwanted Side Reaction of the Hydrothermal Biomass Gasification. Chemical Engineering &Technology 2008:1561–8. doi:10.1002/ceat.200800278.
[24] Titirici M, Antonietti M. Chemistry and materials options of sustainable carbon materials made by hydrothermal carbonization. Chemical Society Reviews 2010:103–16. doi:10.1039/b819318p.
[25] Titirici M, Antonietti M, Baccile N. Hydrothermal carbon from biomass: a comparison of the local structure from poly- to monosaccharides and pentoses/hexoses. Green Chemistry 2008;10:1204–12. doi:10.1039/b807009a.
[26] Hashaikeh R, Fang Z, Butler IS, Hawari J, Kozinski JA. Hydrothermal dissolution of willow in hot compressed water as a model for biomass conversion. Fuel 2007;86:1614–22. doi:10.1016/j.fuel.2006.11.005.
[27] Kruse A, Funke A, Titirici M-M. Hydrothermal conversion of biomass to fuels and energetic materials. Current Opinion in Chemical Biology 2013;17:515–21. doi:10.1016/j.cbpa.2013.05.004.
[28] Volpe M, Goldfarb JL, Fiori L. Hydrothermal carbonization of Opuntia ficus-indica cladodes: Role of process parameters on hydrochar properties. Bioresource Technology 2018.
[29] Sevilla M, Fuertes AB. Sustainable porous carbons with a superior performance for CO2 capture. Energy & Environmental Science 2011;1:1765–71. doi:10.1039/c0ee00784f.
[30] Sevilla M, Fuertes AB, Rezan D-C, Titirici M-M. Applications of Hydrothermal Carbon in Modern Nanotechnology. Sustainable Carbon Materials from Hydrothermal Processes, John Wiley & Sons, Ltd; 2013, p. 213–94. doi:10.1002/9781118622179.ch7.
[31] EUROSTAT. Municipal waste statistics: Municipal waste generated by country. 2017.
[32] Reza MT, Becker W, Sachsenheimer K, Mumme J. Hydrothermal carbonization (HTC): Near infrared spectroscopy and partial least-squares regression for determination of selective components in HTC solid and liquid products derived from maize silage. Bioresource Technology 2014;161:91–101. doi:10.1016/j.biortech.2014.03.008.
[33] Fiori L, Basso D, Castello D, Baratieri M. Hydrothermal carbonization of biomass: Design of a batch reactor and preliminary experimental results. Chemical Engineering Transactions 2014;37:55–60.
[34] Jain A, Balasubramanian R, Srinivasan MP. Hydrothermal conversion of biomass waste to activated carbon with high porosity: A review. Chemical Engineering Journal 2016;283:789–805. doi:10.1016/j.cej.2015.08.014.
[35] Hartmann H, Ahring BK. Anaerobic digestion of the organic fraction of municipal solid waste: Influence of co-digestion with manure. Water Research 2005;39:1543–52. doi:10.1016/j.watres.2005.02.001.
[36] Mäkelä M, Benavente V, Fullana A. Hydrothermal carbonization of lignocellulosic biomass: Effect of process conditions on hydrochar properties. Applied Energy 2015;155:576–84. doi:10.1016/j.apenergy.2015.06.022.

[37] Benavente V, Calabuig E, Fullana A. Upgrading of moist agro-industrial wastes by hydrothermal carbonization. Journal of Analytical and Applied Pyrolysis 2015;113:89–98. doi:10.1016/j.jaap.2014.11.004.
[38] Kalderis D, Kotti MS, Méndez A, Gascó G. Characterization of hydrochars produced by hydrothermal carbonization of rice husk. Solid Earth 2014;5:477–83. doi:10.5194/se-5-477-2014.
[39] Coronella CJ, Lynam JG, Reza MT, Uddin MH. Hydrothermal Carbonization of Lignocellulosic Biomass. In: Jin F, editor. Application of Hydrothermal Reactions to Biomass Conversion, Berlin, Heidelberg: Springer Berlin Heidelberg; 2014, p. 275–311. doi:10.1007/978-3-642-54458-3_12.
[40] Funke A, Ziegler F, Berlin TU. Hydrothermal carbonization of biomass: A summary and discussion of chemical mechanisms for process engineering. Biofuels, Bioproducts and Biorefining 2010;4:160–77. doi:10.1002/bbb.
[41] Sevilla M, Fuertes AB. Chemical and Structural Properties of Carbonaceous Products Obtained by Hydrothermal Carbonization of Saccharides. Chemistry - A European Journal 2009;15:4195–203. doi:10.1002/chem.200802097.
[42] Celaya AM, Lade AT, Goldfarb JL. Co-combustion of brewer's spent grains and Illinois No. 6 coal: Impact of blend ratio on pyrolysis and oxidation behavior. Fuel Processing Technology 2015;129:39–51. doi:10.1016/j.fuproc.2014.08.004.
[43] Goldfarb JL, Liu C. Impact of blend ratio on the co-firing of a commercial torrefied biomass and coal via analysis of oxidation kinetics. Bioresource Technology 2013;149:208–15. doi:10.1016/j.biortech.2013.09.053.
[44] Yangali P, Celaya AM, Goldfarb JL. Co-pyrolysis reaction rates and activation energies of West Virginia coal and cherry pit blends. Journal of Analytical and Applied Pyrolysis 2014;108. doi:10.1016/j.jaap.2014.04.015.
[45] Ekpo U, Ross AB, Camargo-Valero MA, Williams PT. A comparison of product yields and inorganic content in process streams following thermal hydrolysis and hydrothermal processing of microalgae, manure and digestate. Bioresource Technology 2015;200:951–60. doi:10.1016/j.biortech.2015.11.018.
[46] Goldfarb JL, Buessing L, Gunn E, Lever M, Billias A, Casoliba E, et al. Novel Integrated Biorefinery for Olive Mill Waste Management: Utilization of Secondary Waste for Water Treatment. ACS Sustainable Chemistry and Engineering 2017;5:876–84. doi:10.1021/acssuschemeng.6b02202.
[47] Teng H, Wei Y. Thermogravimetric Studies on the Kinetics of Rice Hull Pyrolysis and the Influence of Water Treatment. Industrial & Engineering Chemistry Research 1998;5885:3806–11. doi:10.1021/ie980207p.
[48] Mohan D, Pittman CU, Steele PH. Pyrolysis of Wood/Biomass for Bio-oil: A Critical Review. Energy&Fuels 2006;20:848–89. doi:10.1021/ef0502397.
[49] Hassen A, Belguith K, Jedidi N, Cherif A, Cherif M, Boudabous A. Microbial characterization during composting of municipal solid waste. Bioresource Technology 2001;80:217–25. doi:10.1016/S0960-8524(01)00065-7.
[50] Yang J, Wang S, Lorrain M, Rho D, Abokitse K, Lau PCK. Bioproduction of lauryl lactone and 4-vinyl guaiacol as value-added chemicals in two-phase biotransformation systems. Applied Microbiology and Biotechnology 2009;84:867–76. doi:10.1007/s00253-009-2026-4.
[51] Yang J, Lorrain M, Rho D, Lau PCK. Monitoring of Baeyer-Villiger biotransformation kinetics and fingerprinting using ReactIR 4000 spectroscopy. Industrial Biotechnology 2006;2:138–42. doi:10.1089/ind.2006.2.138.
[52] Lunell S, Eriksson LA. Formation of 2-hexene by cationic dimerization of propene: an ab initio and density functional theory study. Theoretical Chemistry Accounts: Theory, Computation, and Modeling (Theoretica Chimica Acta) 1997;97:277–82. doi:10.1007/s002140050262.
[53] Scaglia B, Orzi V, Artola A, Font X, Davoli E, Sanchez A, et al. Odours and volatile organic compounds emitted from municipal solid waste at different stage of decomposition and relationship with biological stability. Bioresource Technology 2011;102:4638–45. doi:10.1016/j.biortech.2011.01.016.
[54] Koelsch CM, Downes TW, Labuza TP. Hexanal Formation via Lipid Oxidation as a Function of Oxygen Concentration: Measurement and Kinetics. Journal of Food Science 1991;56:816–20. doi:10.1111/j.1365-2621.1991.tb05389.x.
[55] Castello D, Kruse A, Fiori L. Low temperature supercritical water gasification of biomass constituents: Glucose/phenol mixtures. Biomass and Bioenergy 2015;73:84–94. doi:10.1016/j.biombioe.2014.12.010.
[56] Kruse A, Henningsen T, Sınağ A, Pfeiffer J. Biomass Gasification in Supercritical Water: Influence of the Dry Matter Content and the Formation of Phenols. Industrial & Engineering Chemistry Research 2003;42:3711–7. doi:10.1021/ie0209430.
[57] Akiya N, Savage PE. Role of Water in Formic Acid Decomposition. AIChe Journal 1998;44:405–15. doi:10.1002/aic.690440217.
[58] Guisnet M, Magnoux P. Organic chemistry of coke formation. Applied Catalysis A:General 2001;212:83–96. doi:10.1016/S0926-860X(00)00845-0.

Table 1. Raw OFMSW and resulting hydrochar properties as a function of process parameters. Compositional analyses performed in duplicate; average values shown (Standard deviations ≤ 1.8 % for proximate and 1.3 % for ultimate analyses); HHVs average of three measurements, standard deviation ≤ 0.6 MJ/kg).

	Temp	Time	B/W	pH	Hydrochar Yield	Proximate analysis (wt% dry basis)			Ultimate analysis (wt% dry basis)				HHV	Energy Yield
	°C	h				VM	FC	Ash	C	H	O	N	(MJ/kg)	
RAW				5.3		80.7	13.9	5.4	52.0	6.7	32.3	3.6	22.0	
120_3_0.15	120	3.0	0.15	4.7	0.879	81.2	14.8	4.0	51.2	6.6	34.7	3.6	21.9	0.88
160_3_0.15	160	3.0	0.15	4.0	0.826	77.9	15.7	6.4	60.1	7.0	22.2	4.3	25.5	0.96
180_3_0.15	180	3.0	0.15	4.0	0.801	73.8	21.9	4.3	64.6	6.9	20.1	4.0	27.4	1.00
200_3_0.15	200	3.0	0.15	4.5	0.743	68.9	22.5	8.6	65.4	7.3	14.6	4.1	28.2	0.95
220_0_0.15	220	0.0	0.15	3.8	0.739	76.3	18.3	5.4	61.6	6.8	21.8	4.3	26.8	0.90
220_0.5_0.15	220	0.5	0.15	4.4	0.679	75.4	19.8	4.8	66.4	7.1	17.5	4.2	28.1	0.87
220_1_0.15	220	1.0	0.15	4.5	0.650	72.2	21.9	5.9	63.7	6.8	19.9	3.7	28.4	0.84
220_3_0.05	220	3.0	0.05	4.7	0.413	65.2	28.9	5.9	67.6	6.6	16.0	3.9	27.9	0.53
220_3_0.10	220	3.0	0.10	4.6	0.414	68.6	26.8	4.6	68.6	6.8	16.2	3.8	29.2	0.55
220_3_0.15	220	3.0	0.15	4.6	0.639	69.5	24.7	5.8	67.1	6.6	16.2	4.3	29.4	0.86
220_3_0.20	220	3.0	0.20	4.6	0.607	69.4	26.1	4.5	69.2	7.0	15.3	3.9	29.6	0.82
220_3_0.25	220	3.0	0.25	4.6	0.602	67.9	27.1	5.0	68.9	7.1	15.1	3.9	29.6	0.81
220_5_0.15	220	5.0	0.15	4.6	0.612	69.1	25.8	5.1	69.4	7.2	14.3	4.0	30.1	0.84
220_6_0.15	220	6.0	0.15	4.6	0.557	66.9	27.3	5.8	69.6	7.0	13.6	3.9	29.8	0.76
240_3_0.15	240	3.0	0.15	4.7	0.477	68.4	26.9	4.7	71.6	7.2	12.4	4.1	31.5	0.68
260_3_0.15	260	3.0	0.15	5.0	0.562	68.5	28.6	2.9	73.5	7.8	11.8	4.0	31.9	0.82
280_3_0.15	280	3.0	0.15	6.3	0.563	63.9	31.8	4.3	73.7	7.0	11.0	4.0	32.5	0.83

Table 2. OLS Multivariate linear regression of impact of reaction temperature, time and biomass to water ratio on hydrochar characteristics

	Hydrochar Yield (wt%)	HHV (MJ/kg)	Energy Yield (%)	Volatile Matter (wt%)	Fixed Carbon (wt%)	Carbon (wt%)	Oxygen (wt%)
Temperature	-0.003**	0.066**	-0.001	-0.001**	0.001**	0.138**	-0.137**
(°C)	(0.001)	(0.004)	(0.001)	(0.000)	(0.000)	(0.012)	(0.016)
Time	-0.024	0.466**	-0.018	-0.015**	0.015**	1.190**	-1.208*
(h)	(0.015)	(0.110)	(0.019)	(0.004)	(0.003)	(0.307)	(0.416)
B/W	1.141	7.600	1.660*	0.124	-0.086	6.400	-5.400
	(0.529)	(3.919)	(0.681)	(0.136)	(0.123)	(10.969)	(14.868)
Constant	1.110**	12.178**	0.899**	0.953**	-0.024	32.603**	50.706**
	(0.156)	(1.154)	(0.200)	(0.040)	(0.036)	(3.229)	(4.377)
R-squared	0.688	0.951	0.430	0.828	0.865	0.918	0.856
Observations	17	17	17	17	17	17	17

Standard errors in parentheses ** p<0.01, * p<0.05

Table 3. Yields and heating values of extractable and non-extractable hydrochar portions (HTC reaction time: 3 h; B/W=0.15)

HTC Temp (°C)	Hydrochar Yield	HHV hydrochar (MJ/kg)	Non-Extractable Char (wt%)	HHV Non-Extractable Char (MJ/kg)	Extractable Char (wt%)	HHV Extractable Char (MJ/kg)	Predicted HHV hydrochar (MJ/kg)	HHV Deviation from Measured
220	0.639	29.4	59.6	25.2	40.4	34.5	28.9	-1.6%
240	0.477	31.5	45.4	27.0	54.6	35.4	31.6	0.3%
260	0.562	31.9	65.7	28.6	34.3	35.9	31.1	-2.5%
280	0.563	32.5	65.1	29.5	34.9	36.5	31.9	-1.6%

Table 4. GCMS analysis of "secondary char" extracted from OFMSW hydrochars normalized to gram of solid hydrochar (mg/g_{solid} for "marker" compounds; TIC, Total Ion Count for observed but not calibrated compounds); error on concentration < 5 ppm

Retention Time (min)	Compound	**Raw OFMSW**	**120_3_0.15**	**220_1_0.15**	**220_3_0.15**	**220_6_0.15**	**260_3_0.15**
			Normalized Concentration (mg/g_{solid})				
10.4	2-furancarboxaldehyde (furfural)			0.208	0.981		0.165
13.9	2-furanmethanol						3.254
15.7	Styrene		2.756				
29.6	Maltol						0.398
44.4	Vanillin					2.889	1.965
25.6-25.9	Phenol		0.422	0.563	2.357	2.898	4.440
35.2-35.6	5-hydroxymethylfurfural			4.039	3.614	3.675	2.482
40.9-41.1	Syringol				1.647		
41.1-41.3	Eugenol			1.202			
63.5-63.8	Octadecanoic acid			87.562	74.569	60.730	10.158
			Normalized Area (TIC/g_{solid})				
8.9-9.0	1,4-butanediol		1.236E+05				
9.1	Hexanal	4.189E+04	5.807E+05				
9.2	Pentanal	8.829E+02	8.918E+03	2.151E+04			
11.7	2-hexene	1.363E+03	8.865E+04				
11.9	Lauryl lactone	5.602E+03	2.302E+04				
36.9	Furan,2-ethyl-5-methyl-		2.101E+05				
63.7	Hexadecanoic Acid			1.876E+05	1.212E+06	1.375E+06	7.653E+04
56.9-57.0	Levoglucosan			9.931E+03	1.185E+05	1.301E+05	
68.8-68.9	2-Acetylfuran			6.530E+04	1.409E+05	9.230E+04	4.743E+04
69.0-69.1	Oxacyclotridecan-2-one			3.404E+05	2.127E+06	4.045E+06	6.418E+04

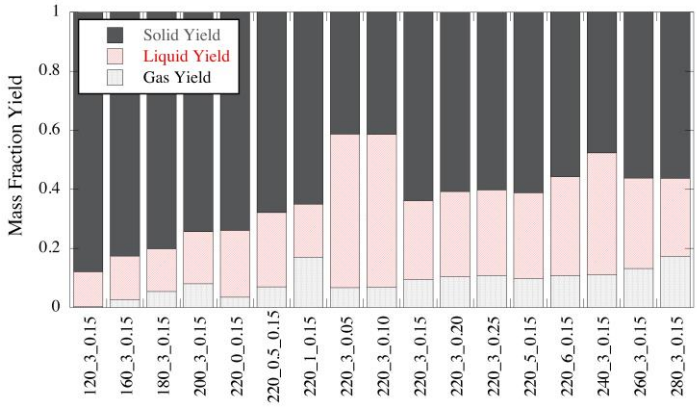

a. Weight fraction distribution of hydrothermally carbonized OFMSW in solid, liquid and gas phases (liquid determined via difference)

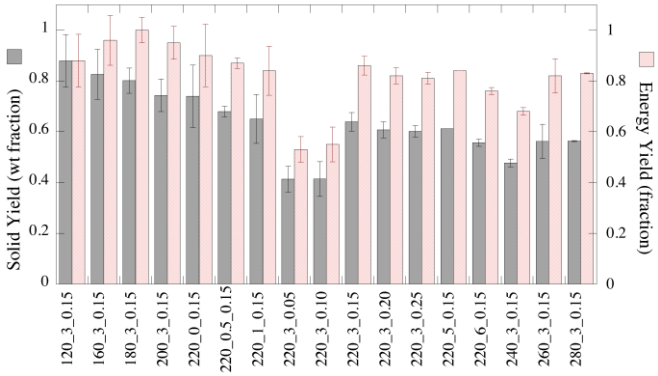

b. Solid and energy yields (error bars indicate 95% confidence interval)

Figure 1. Product distribution and energy yields for hydrothermal carbonization of OFMSW at varying temperatures, residence times and B/W ratios

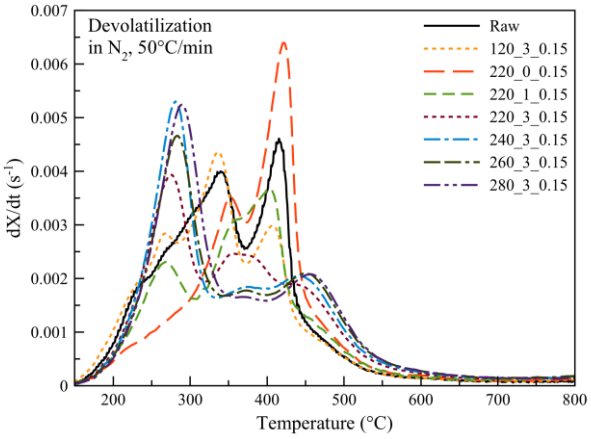

a. Pyrolysis in N_2

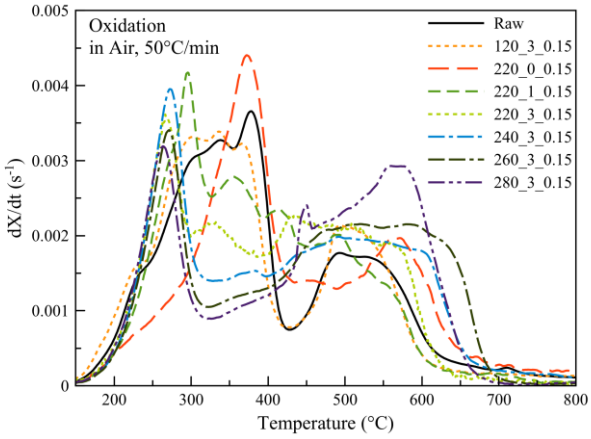

b. Oxidation in air

Figure 2. Derivative thermogravimetric curves for raw OFMSW and hydrochars pyrolyzed and oxidized at 50 °C/min

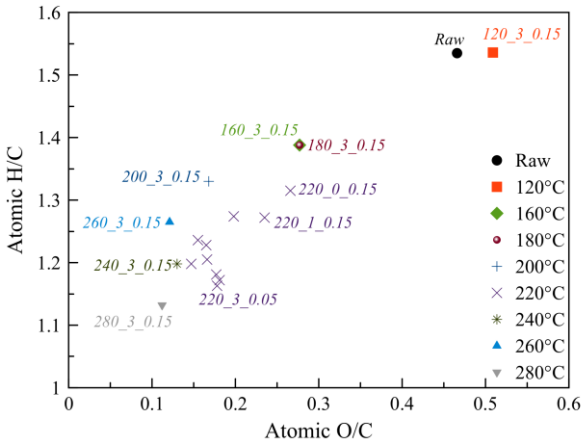

a. van Krevelen diagram

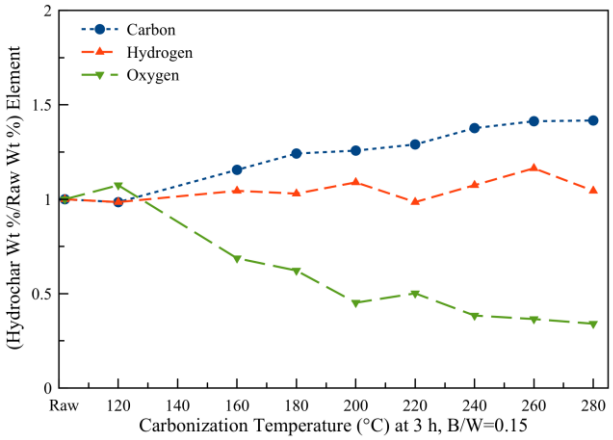

b. Elemental distribution as a function of reaction temperature in terms of hydrochar composition/raw OFMSW composition

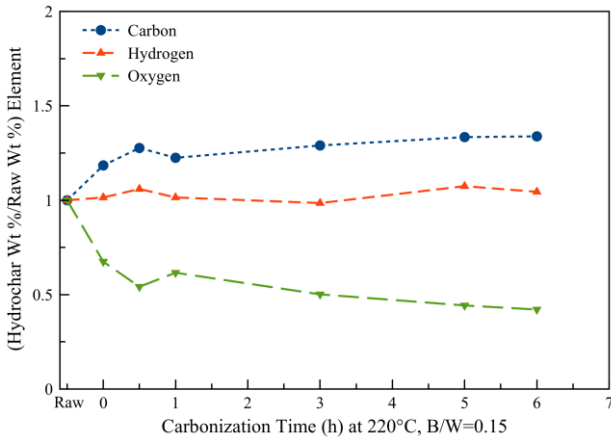

c. Elemental distribution as a function of reaction time in terms of hydrochar composition/raw OFMSW composition

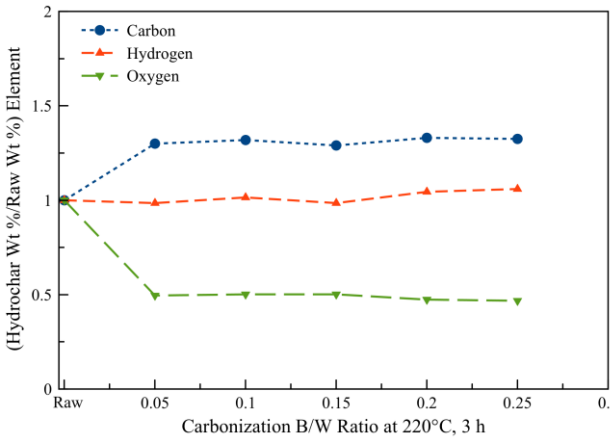

d. Elemental distribution as a function of B/W in terms of hydrochar composition/raw OFMSW composition

Figure 3. Impact of HTC processing conditions on elemental composition of hydrochars

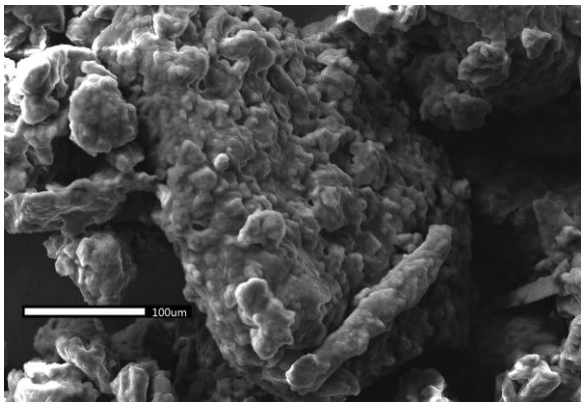

a. Raw OFMSW

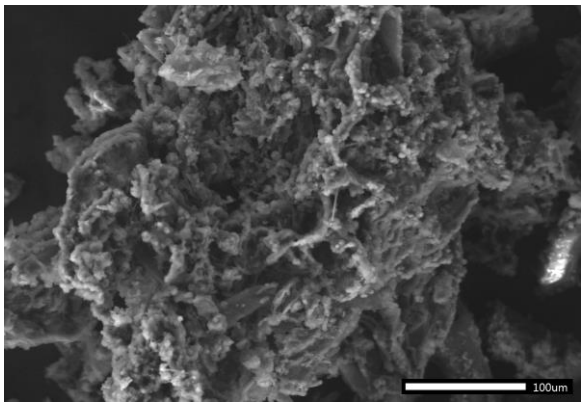

b. 180_3_0.15

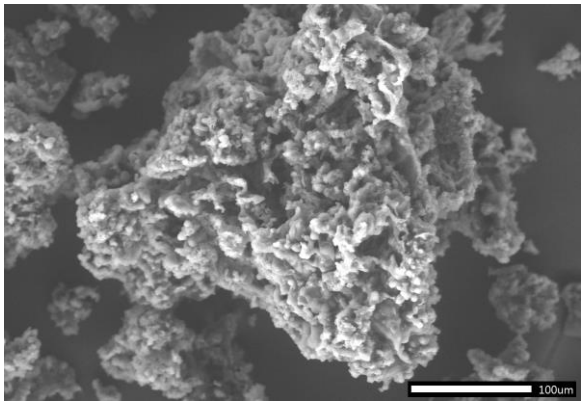

c. 240_3_0.15

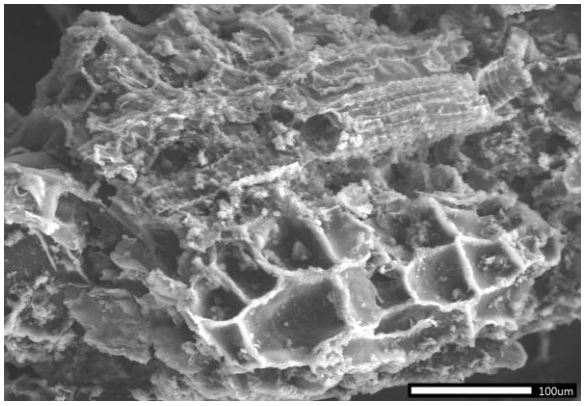

d. 240_3_0.15_extracted

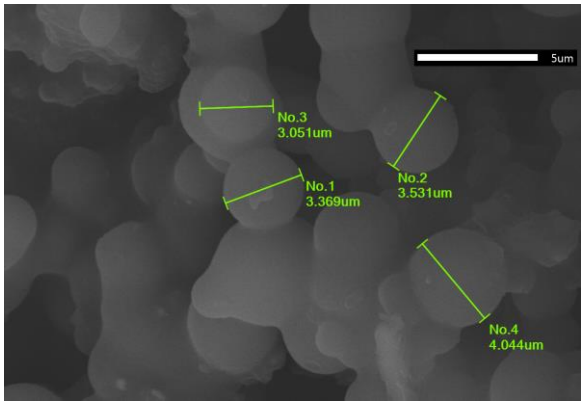

e. 280_3_0.15 (5000x magnification; scale bar = 5 μm to highlight secondary char spheres)

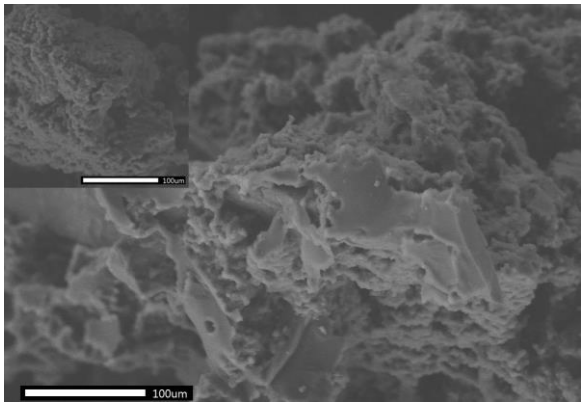

f. 280_3_0.15_extracted with inset image of 280_3_0.15 primary char

Figure 4. SEM images of OFMSW raw, hydrochars and extracted hydrochars at 250x magnification, scale bar = 100 μm

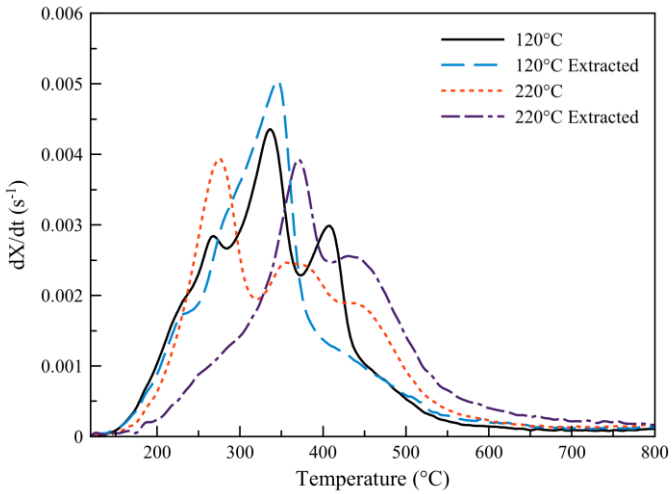

a. Low-temperature hydrochars in nitrogen, 50 °C/min

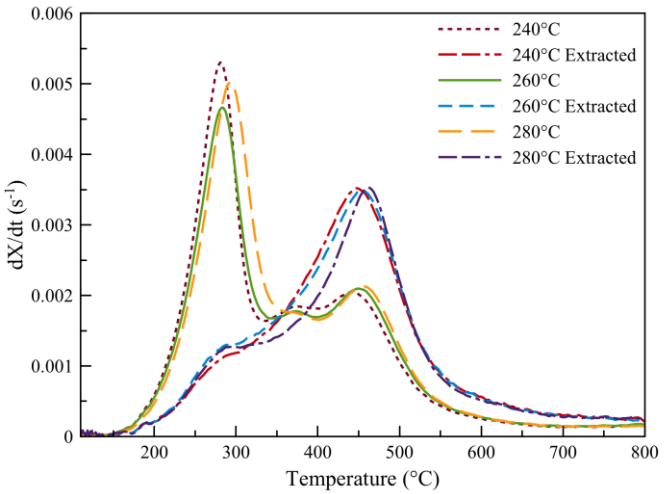

b. High-temperature hydrochars in nitrogen, 50 °C/min

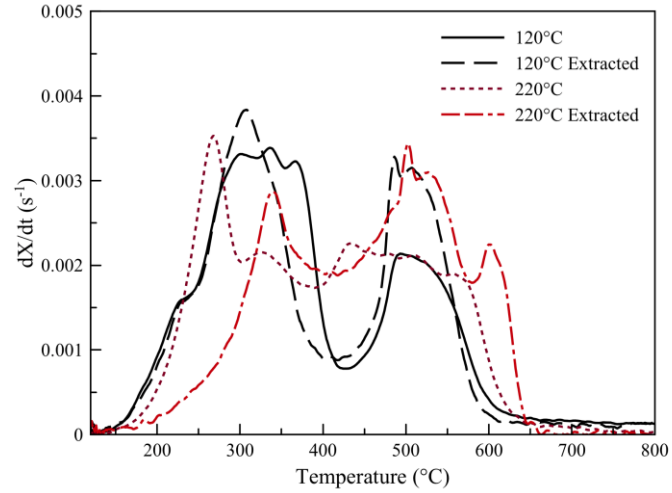

c. Low-temperature hydrochars in air, 50 °C/min

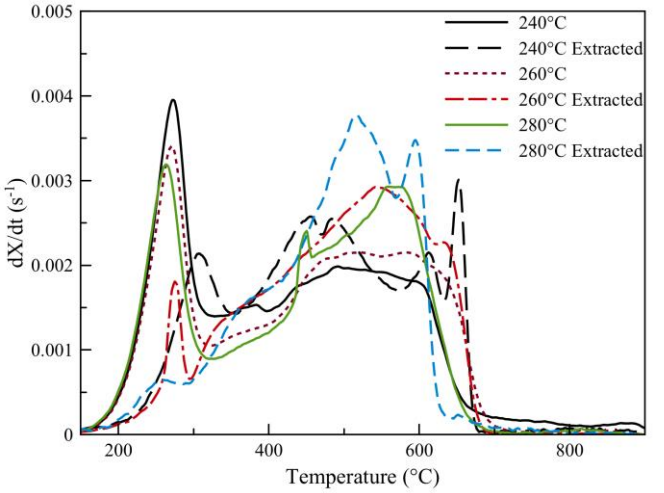

d. High-temperature hydrochars in air, 50 °C/min

Figure 5. DTG curves of hydrochars prepared at B/W=0.15 over three hours between 120 and 280 °C, pre- and post- solvent extraction